

Pyrazolium salts as a new class of ionic liquid crystals†

Ignacio Sánchez,^a José Antonio Campo,^a José Vicente Heras,^a M. Rosario Torres^b and Mercedes Cano^{*a}

Received 28th March 2012, Accepted 14th May 2012

DOI: 10.1039/c2jm31939j

New alkyloxyphenyl substituted pyrazolium salts $[\text{H}_2\text{pz}^{\text{R}(n)}][\text{A}]$ ($\text{R}(n) = \text{C}_6\text{H}_4\text{OC}_n\text{H}_{2n+1}$; $n = 8, 10, 12, 14, 16, 18$; $[\text{A}] = \text{Cl}^-, \text{BF}_4^-, \text{ReO}_4^-, \text{SbF}_6^-, \text{CF}_3\text{SO}_3^-, \text{CH}_3\text{-}p\text{-C}_6\text{H}_4\text{SO}_3^-$) have been synthesised and characterised. Those containing Cl^- , BF_4^- , ReO_4^- and SbF_6^- anions behave as liquid crystal compounds exhibiting smectic A (SmA) mesophases. Because the precursor neutral pyrazoles $[\text{Hpz}^{\text{R}(n)}]$ were not liquid crystals, their protonation and strategic choice of the counter-anion was found useful to achieve mesomorphism and to modulate the transition temperatures, so giving rise to a new class of ionic liquid crystals. The X-ray crystal structures of selected derivatives as representative examples of each type of compound have been resolved. In most of the cases, for X-ray purposes, the salts were designed to contain one methoxyphenyl-substituted pyrazolium cation. Different structural features have been found depending on the nature of the anion. Dimeric units held through hydrogen bonds are arranged in chains which pack in a layer-like array for compounds $[\text{H}_2\text{pz}^{\text{R}(10)}][\text{BF}_4]$, $[\text{H}_2\text{pz}^{\text{R}(1)}][\text{OTf}]$ and $[\text{H}_2\text{pz}^{\text{R}(1)}][\text{PTS}]$, but 2D structures were found for $[\text{H}_2\text{pz}^{\text{R}(1)}][\text{Cl}]$ and $[\text{H}_2\text{pz}^{\text{R}(1)}][\text{ReO}_4]$. Relationships between the solid and the mesophase structures are proposed. The absence of mesomorphism for CF_3SO_3^- and $\text{CH}_3\text{-}p\text{-C}_6\text{H}_4\text{SO}_3^-$ derivatives is also explained on the basis of the main structural features.

Introduction

Ionic liquid crystals (ILCs) can be considered as an extension of the typical ionic liquid materials (organic salts with melting temperatures lower than 100 °C).¹ In addition to their characteristic ionic liquid properties (low vapour pressure, thermal stability, polarity, electric behaviour, *etc.*),^{1,2} they exhibit liquid crystal properties, such as molecular orientational order.^{2,3} Alternatively, ILCs can be regarded as a class of liquid crystals constituted by cations and anions.^{3,4} Due to their dual behaviour as liquid crystals and ionic liquids, they offer new opportunities as ion conductive materials⁵⁻⁷ in electronic devices, as organised reaction media⁸ and as template agents in materials science⁹ or in bio-related science.^{10,11}

Examples of ILC materials include ammonium, phosphonium, pyridinium, pyrrolidinium and imidazolium salts,^{2-6,10-23} the latter of these being the most abundantly studied because of the profuse applications of related imidazolium-based ionic liquids.^{2,3,12} In all the above examples the cationic group acts as

the mesogenic core and their thermal properties have been described and occasionally compared.

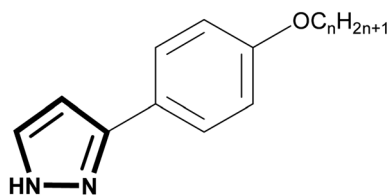
Differences in mesophase range, thermal stability and clearing temperature have been observed depending on variables such as the chain length or the nature of the cation and anion present in the salts.^{2-4,11,13} For instance, the mesophase stability range of imidazolium and pyridinium salts was increased by increasing the chain length, however, the clearing points were dependant on the cation or the anion.^{3,13-15} At the same time, the melting points were strongly dependent on the choice of counterion, and imidazolium salts with fluorinated anions exhibited the lowest melting temperatures.³ As a consequence, it seems to be important to highlight that the thermal behaviour of different ILCs does not follow the same pattern when modifying the same variables, therefore a systematic study is required for each new family of ionic salts investigated.

We are now involved in the study of a new class of ILC based on pyrazolium salts, taking into account our experience on liquid crystalline pyrazole complexes. In addition, from the best of our knowledge, ILCs based on pyrazolium salts have not been described yet. Previous work from our lab has been directed towards the design, preparation and study of liquid crystal properties of metallomesogens containing pyrazole ligands of the types 3-(4-alkyloxyphenyl)pyrazole, $[\text{Hpz}^{\text{R}(n)}]$ and 3,5-di(4-alkyloxyphenyl)pyrazole, $[\text{Hpz}^{2\text{R}(n)}]$, ($\text{R}(n) = \text{C}_6\text{H}_4\text{OC}_n\text{H}_{2n+1}$; $n = 4-18$) (Scheme 1),²⁴⁻²⁷ most of them being ILCs in which the metallorganic moieties are the mesogenic groups. In particular, the ionic complexes of the type $[\text{M}(\text{Hpz}^{\text{R}(n)})_2][\text{A}]$ and $[\text{M}(\text{Hpz}^{2\text{R}(n)})_2][\text{A}]$ ($\text{M} = \text{Ag}, \text{Au}$; $\text{A} = \text{NO}_3^-, \text{BF}_4^-, \text{PF}_6^-$,

^aDepartamento de Química Inorgánica I, Facultad de Ciencias Químicas, Universidad Complutense, 28040 Madrid, Spain. E-mail: mmcano@quim.ucm.es; Fax: +34 91 394 4352; Tel: +34 91 394 4340

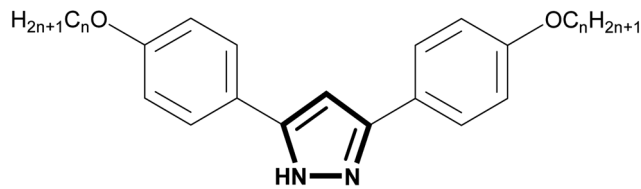
^bCAI de Difracción de Rayos-X, Facultad de Ciencias Químicas, Universidad Complutense, 28040 Madrid, Spain

† Electronic supplementary information (ESI) available: Characterisation of compounds, Table S1–S6 and Fig. S1. CCDC reference numbers 873375–873379 for compounds **Cl-1**, **BF₄-10**, **ReO₄-1**, **OTf-1** and **PTS-1**. For ESI and crystallographic data in CIF or other electronic format see DOI: 10.1039/c2jm31939j



$n = 4, 6, 8, 10, 12, 14, 16, 18$

[Hpz^{R(n)}]



$n = 4, 6, 8, 10, 12, 14, 16, 18$

[Hpz^{2R(n)}]

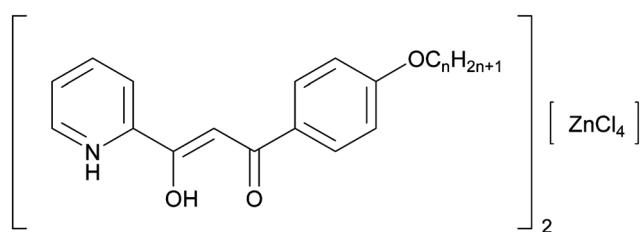
Scheme 1 Pyrazole-type ligands.

CF_3SO_3^- , $\text{CH}_3\text{-}p\text{-C}_6\text{H}_4\text{SO}_3^-$)^{28,29} have been shown to exhibit monotropic or enantiotropic smectic behaviour and present an extensive range of stability of the mesophases. In addition, it was also proved that the free 3,5-alkoxyphenyl-disubstituted pyrazoles are mesomorphic^{26,30} in contrast to the absence of mesomorphism of the related 3(5)-monosubstituted ligands.^{24,25}

We have also investigated new ILC salts containing β -diketonilpyridinium cations with $[\text{ZnCl}_4]^-$ anions (Scheme 2), which exhibit enantiotropic smectic behaviour with a wide mesophase range.³¹

Encouraged by these results, we are now interested in the design of new ILCs based on cations produced by protonation of the non-mesomorphic monosubstituted pyrazoles $[\text{Hpz}^{\text{R}(n)}]$. These cations should be combined with different counterions in order to study the potential for inducing and tuning the mesomorphism in the promesogenic moiety as a function of the anion characteristics and/or the alkyl lateral chain length.

In this work we present the synthesis and mesomorphic properties of new ionic liquid crystals based on pyrazolium cations of the type $[\text{H}_2\text{pz}^{\text{R}(n)}]^+$ bearing one alkoxyphenyl substituent of variable chain length ($n = 8\text{--}18$ carbon atoms) at the position 3(5) of the pyrazole ring. We have used six different counterions, Cl^- , BF_4^- , ReO_4^- , SbF_6^- , CF_3SO_3^- (OTf) and $\text{CH}_3\text{-}p\text{-C}_6\text{H}_4\text{SO}_3^-$ (PTS) for each cationic unit, so extending our study to six families of compounds I–VI (Scheme 3), four of them exhibiting mesomorphism.



[HOOR^{R(n)}pyH]₂[ZnCl₄]

Scheme 2 β -Diketonilpyridinium-based ILC.

Experimental

Materials and physical measurements

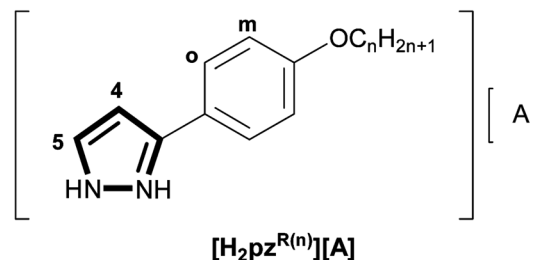
All commercial reagents were used as supplied. The precursor pyrazoles $[\text{Hpz}^{\text{R}(n)}]$ ($\text{R}(n) = \text{C}_6\text{H}_4\text{OC}_n\text{H}_{2n+1}$; $n = 1, 8, 10, 12, 14, 16, 18$) were prepared following a general procedure previously reported by us.^{24,25}

Elemental analyses for carbon, hydrogen, nitrogen and sulfur were carried out by the Microanalytical Service of Complutense University (validated range: %C 0.5–94.7, %H 0.5–7.6, %N 0.5–23.0 and %S 0.5–30.6). IR spectra were recorded on a FTIR Thermo Nicolet 200 spectrophotometer with samples as KBr pellets in the 4000–400 cm^{-1} region. $^1\text{H-NMR}$ spectra were performed at room temperature on a Bruker DPX-300 spectrophotometer (NMR Service of Complutense University) from solutions in $(\text{CD}_3)_2\text{CO}$ or CDCl_3 . Chemical shifts (δ) are listed relative to Me_4Si using the signal of the deuterated solvent as the reference (2.05 and 7.26 ppm, respectively), and coupling constants (J) are in hertz. Multiplicities are indicated as s (singlet), d (doublet), t (triplet), m (multiplet), br s (broad signal). The ^1H chemical shifts and coupling constants are accurate to ± 0.01 ppm and ± 0.3 Hz, respectively. Scheme 3 shows the nomenclature used for the NMR assignments.

Phase studies were carried out by optical microscopy using an Olympus BX50 microscope equipped with a Linkam THMS 600 heating stage. The temperatures were assigned on the basis of optic observations with polarised light. Measurements of the transition temperatures were made using a Perkin Elmer Pyris 1 differential scanning calorimeter with the sample (1–4 mg) sealed hermetically in aluminium pans and with a heating or cooling rate of 5–10 K min^{-1} . The X-ray diffractograms at variable temperature were recorded on a Panalytical X'Pert PRO MPD diffractometer in a $\theta\text{--}\theta$ configuration equipped with an Anton Paar HTK1200 heating stage (X-Ray Diffraction Service of Complutense University).

Pyrazolium compounds of the type $[\text{H}_2\text{pz}^{\text{R}(n)}][\text{A}]$ ($\text{A} = \text{Cl}^-$, BF_4^- ; $\text{R}(n) = \text{C}_6\text{H}_4\text{OC}_n\text{H}_{2n+1}$, $n = 1, 8, 10, 12, 14, 16, 18$)

To a solution of 3 mmol of the corresponding $[\text{Hpz}^{\text{R}(n)}]$ in dichloromethane (50 mL), a hydrochloric acid solution (spec. grav. 1.19) or $\text{HBF}_4 \cdot \text{Et}_2\text{O}$ was added until a white or pale yellow precipitate was formed. The mixture was stirred for 3 hours and



[H₂pz^{R(n)}][A]

$\text{R}(n) = \text{C}_6\text{H}_4\text{OC}_n\text{H}_{2n+1}$; $n = 8, 10, 12, 14, 16, 18$

$[\text{A}] = \text{Cl}^-, \text{BF}_4^-, \text{ReO}_4^-, \text{SbF}_6^-, \text{CF}_3\text{SO}_3^-, \text{CH}_3\text{-}p\text{-C}_6\text{H}_4\text{SO}_3^-$

Scheme 3 Pyrazolium salts studied in this work, and atom numbering used in the NMR assignments.

then cooled to $-18\text{ }^{\circ}\text{C}$. The solid was filtered, washed with water and dried *in vacuo*. All compounds were characterised by IR and $^1\text{H-NMR}$ spectroscopies and CHN analyses (deposited as ESI †). Specific examples of the characterisation are given below.

$[\text{H}_2\text{pz}^{\text{R}(\text{s})}][\text{Cl}]$ (Cl-8**):** colourless solid (80%). Elemental analysis: found: C, 65.8; H, 7.8; N, 9.1%. $\text{C}_{17}\text{H}_{25}\text{N}_2\text{OCl}$ requires C, 66.1; H, 8.2; N, 9.1%. $\nu_{\text{max}}(\text{KBr})/\text{cm}^{-1}$: 3144, 3080 $\nu(\text{NH})$, 1615 $\nu(\text{C}=\text{C} + \text{C}=\text{N})$. δ_{H} (300 MHz; CDCl_3 ; Me_4Si): 0.89 (3 H, t, J 6.7, CH_3), 1.30 (10 H, m, CH_2), 1.81 (2 H, m, CH_2), 4.01 (2 H, t, J 6.7, OCH_2), 6.71 (1 H, d, J 2.8, H4), 7.02 (2 H, d, J 8.9, H_m), 7.90 (1 H, d, J 2.8, H5), 7.93 (2 H, d, J 8.9, H_o).

$[\text{H}_2\text{pz}^{\text{R}(\text{s})}][\text{BF}_4]$ (BF₄-8**):** pale yellow solid (69%). Elemental analysis: found: C, 57.0; H, 6.9; N, 7.8%. $\text{C}_{17}\text{H}_{25}\text{N}_2\text{OBF}_4$ requires C, 56.7; H, 7.0; N, 7.8%. $\nu_{\text{max}}(\text{KBr})/\text{cm}^{-1}$: 3385, 3241 $\nu(\text{NH})$, 1615 $\nu(\text{C}=\text{C} + \text{C}=\text{N})$, 1083 $\nu(\text{B-F})$. δ_{H} (300 MHz; CDCl_3 ; Me_4Si): 0.89 (3 H, t, J 6.7, CH_3), 1.30 (10 H, m, CH_2), 1.81 (2 H, m, CH_2), 4.02 (2 H, t, J 6.7, OCH_2), 6.81 (1 H, d, J 2.8, H4), 7.02 (2 H, d, J 8.9, H_m), 7.67 (2 H, d, J 8.9, H_o), 8.14 (1 H, d, J 2.8, H5), 12.83 (br s, NH), 13.27 (br s, NH).

Pyrazolium compounds of the type $[\text{H}_2\text{pz}^{\text{R}(\text{m})}][\text{A}]$ ($\text{A} = \text{ReO}_4^-$, SbF_6^- , OTf, PTS; $\text{R}(n) = \text{C}_6\text{H}_4\text{OC}_n\text{H}_{2n+1}$, $n = 1, 8, 10, 12, 14, 16, 18$)

To a solution of the $[\text{H}_2\text{pz}^{\text{R}(\text{m})}][\text{Cl}]$ in 40 mL of CH_2Cl_2 the corresponding salt AgA ($\text{A} = \text{ReO}_4^-$, SbF_6^- , OTf, PTS) in 8 : 2 mL of $\text{CH}_2\text{Cl}_2\text{-CH}_3\text{CN}$ and in a 1 : 1 molar ratio was added, under a nitrogen atmosphere. The mixture was stirred for 24 hours in the absence of light and then filtered through Celite $^{\text{®}}$. The clear filtrate was concentrated *in vacuo* until a solid precipitated. The white solid was filtered and dried *in vacuo*. All compounds were characterised by IR and $^1\text{H-NMR}$ spectroscopies and CHN or CHNS analyses (deposited as ESI †). A specific example of the characterisation for a compound of each family is given below.

$[\text{H}_2\text{pz}^{\text{R}(\text{s})}][\text{ReO}_4]$ (ReO₄-8**):** colourless solid (75%). Elemental analysis: found: C, 38.7; H, 4.8; N, 5.4%. $\text{C}_{17}\text{H}_{25}\text{N}_2\text{O}_5\text{Re}$ requires C, 39.0; H, 4.8; N, 5.4%. $\nu_{\text{max}}(\text{KBr})/\text{cm}^{-1}$: 3144, 3124 $\nu(\text{NH})$, 1616 $\nu(\text{C}=\text{C} + \text{C}=\text{N})$, 908 $\nu(\text{Re-O})$. δ_{H} (300 MHz; CDCl_3 ; Me_4Si): 0.89 (3 H, t, J 6.7, CH_3), 1.29 (10 H, m, CH_2), 1.81 (2 H, m, CH_2), 4.02 (2 H, t, J 6.7, OCH_2), 6.79 (1 H, d, J 2.3, H4), 7.04 (2 H, d, J 8.7, H_m), 7.72 (2 H, d, J 8.7, H_o), 7.93 (1 H, d, J 2.3, H5).

$[\text{H}_2\text{pz}^{\text{R}(\text{s})}][\text{SbF}_6]$ (SbF₆-8**):** colourless solid (49%). Elemental analysis: found: C, 40.5; H, 4.9; N, 5.6%. $\text{C}_{17}\text{H}_{25}\text{N}_2\text{OSbF}_6$ requires C, 40.1; H, 5.0; N, 5.5%. $\nu_{\text{max}}(\text{KBr})/\text{cm}^{-1}$: 3336, 3167 $\nu(\text{NH})$, 1616 $\nu(\text{C}=\text{C} + \text{C}=\text{N})$, 665 $\nu(\text{Sb-F})$. δ_{H} (300 MHz; CDCl_3 ; Me_4Si): 0.90 (3 H, t, J 6.7, CH_3), 1.30 (10 H, m, CH_2), 1.81 (2 H, m, CH_2), 4.01 (2 H, t, J 6.7, OCH_2), 6.74 (1 H, d, J 2.4, H4), 7.01 (2 H, d, J 8.3, H_m), 7.63 (2 H, d, J 8.3, H_o), 7.87 (1 H, d, J 2.4, H5).

$[\text{H}_2\text{pz}^{\text{R}(\text{s})}][\text{OTf}]$ (OTf-8**):** colourless solid (75%). Elemental analysis: found: C, 50.9; H, 5.8; N, 6.6; S, 7.6%. $\text{C}_{18}\text{H}_{25}\text{N}_2\text{SO}_4\text{F}_3$ requires C, 51.2; H, 6.0; N, 6.6; S, 7.6%. $\nu_{\text{max}}(\text{KBr})/\text{cm}^{-1}$: 3136 $\nu(\text{NH})$, 1618 $\nu(\text{C}=\text{C} + \text{C}=\text{N})$, 1257, 1032 $\nu(\text{SO})$. δ_{H} (300 MHz; CDCl_3 ; Me_4Si): 0.90 (3 H, t, J 6.7, CH_3), 1.30 (10 H, m, CH_2), 1.82 (2 H, m, CH_2), 4.03 (2 H, t, J 6.7, OCH_2), 6.79 (1 H, d, J 2.8, H4), 7.03 (2 H, d, J 8.8, H_m), 7.70 (2 H, d, J 8.8, H_o), 8.11 (1 H, d, J 2.8, H5), 13.67 (br s, NH), 14.51 (br s, NH).

$[\text{H}_2\text{pz}^{\text{R}(\text{s})}][\text{PTS}]$ (PTS-8**):** colourless solid (85%). Elemental analysis: found: C, 64.7; H, 7.1; N, 6.3; S, 7.1%. $\text{C}_{24}\text{H}_{32}\text{N}_2\text{SO}_4$ requires C, 64.8; H, 7.2; N, 6.3; S, 7.2%. $\nu_{\text{max}}(\text{KBr})/\text{cm}^{-1}$: 3218, 3136 $\nu(\text{NH})$, 1617 $\nu(\text{C}=\text{C} + \text{C}=\text{N})$, 1186, 1021 $\nu(\text{SO})$. δ_{H} (300 MHz; CDCl_3 ; Me_4Si): 0.89 (3 H, t, J 6.7, CH_3), 1.29 (10 H, m, CH_2), 1.80 (2 H, m, CH_2), 2.36 (3 H, s, $\text{CH}_3(\text{PTS})$), 3.99 (2 H, t, J 6.7, OCH_2), 6.70 (1 H, d, J 2.7, H4), 6.97 (2 H, d, J 8.7, H_m), 7.20 (2 H, d, J 8.1, $\text{H}_o(\text{PTS})$), 7.73 (2 H, d, J 8.7, H_o), 7.84 (2 H, d, J 8.1, $\text{H}_m(\text{PTS})$), 8.05 (1 H, d, J 2.7, H5).

Crystallographic structure determinations

Data collection for all compounds was carried out at room temperature on a Bruker Smart CCD diffractometer using graphite-monochromated Mo-K_{α} radiation ($\lambda = 0.71073\text{ \AA}$) operating at 50 kV and 35 mA for **Cl-1** and **BF₄-10** and at 50 kV and 30 mA for **ReO₄-1**, **OTf-1** and **PTS-1**. In all cases, the data were collected over a hemisphere of the reciprocal space by combination of three exposure sets. Each exposure was 20 s long for **Cl-1**, **BF₄-10**, **ReO₄-1** and **OTf-1** and 10 s for **PTS-1**, and covered 0.3° in ω . The first 100 frames were recollected at the end of the data collection to monitor crystal decay, and no appreciable decay was observed. A summary of the fundamental crystal and refinement data is given in Table 1.

The structures were solved by direct methods and refined by full-matrix least-square procedures on F^2 .³² All non-hydrogen atoms were refined anisotropically. All hydrogen atoms were included in calculated positions and refined riding on the respective carbon atoms, with some exceptions. The hydrogens H1 and H2 bonded to N1 and N2 atoms for **Cl-1**, **BF₄-10** and **OTf-1**, and H1, H2, H3, H4, H5 and H6 bonded to N1, N2, N3, N4, N5 and N6, respectively, for **PTS-1** were located in a Fourier synthesis and refined riding on the respective bonded atoms. For compound **ReO₄-1**, they were located in a Fourier synthesis and fixed.

Results and discussion

$^1\text{H-NMR}$ and IR characterisation

Table 2 depicts all the new ionic salts prepared in this work including the family and the nomenclature used according to the counterion and the number of carbon atoms in the alkyl chain. All compounds were characterised by elemental analysis and spectroscopic techniques (IR and $^1\text{H-NMR}$; see Experimental section and ESI †).

The $[\text{H}_2\text{pz}^{\text{R}(\text{m})}][\text{A}]$ salts were prepared in two different ways (a and b) according to Scheme 4. Chloride and tetrafluoroborate derivatives (**I** and **II**) were obtained by protonation of the pyrazole precursor with hydrochloric (a_1) or tetrafluoroboric (a_2) acid, respectively. The metathesis reactions (b) of the corresponding pyrazolium chlorides (**I**) with silver perrhenate, silver hexafluoroantimonate, silver trifluoromethanesulfonate (OTf) and silver *p*-toluenesulfonate (PTS) in a 1 : 1 molar ratio in CH_2Cl_2 gave rise to the new salts **III**, **IV**, **V** and **VI**, respectively.

The $^1\text{H-NMR}$ spectra of the new salts (**I-VI**) in CDCl_3 solution at room temperature display the expected signals from the pyrazolium and alkyloxyphenyl groups. Compound **VI** exhibits, in addition, the signals for the protons of the PTS counteranion. In all cases the NH signals are not observed (except for

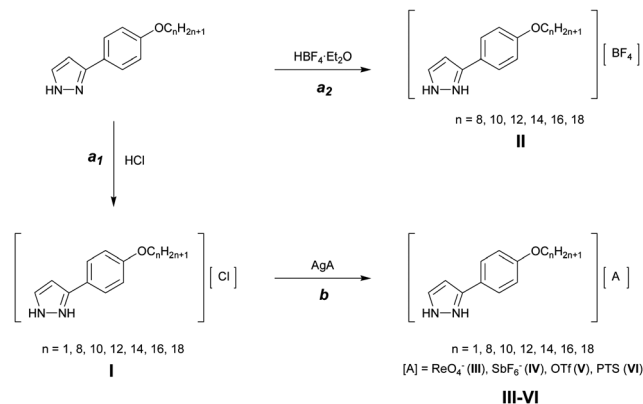
Table 1 Crystal and refinement data for Cl-1, BF₄-10, ReO₄-1, OTf-1 and PTS-1

	Cl-1	BF ₄ -10	ReO ₄ -1	OTf-1	PTS-1
Empirical formula	C ₁₀ H ₁₁ ClN ₂ O	C ₁₉ H ₂₉ BF ₄ N ₂ O	C ₁₀ H ₁₁ N ₂ O ₅ Re	C ₁₁ H ₁₁ F ₃ N ₂ O ₄ S	C ₁₇ H ₁₈ N ₂ O ₄ S
Formula weight	210.66	388.25	425.41	324.28	346.39
Crystal system	Orthorhombic	Triclinic	Orthorhombic	Triclinic	Triclinic
Space group	<i>Pbca</i>	<i>P</i> (1)	<i>P2</i> ₁ <i>2</i> ₁ <i>2</i> ₁	<i>P</i> (1)	<i>P</i> (1)
Space group number	61	2	19	2	2
<i>a</i> /Å	11.998(2)	6.1620(6)	4.9991(4)	6.344(4)	9.993(2)
<i>b</i> /Å	7.316(2)	9.2230(9)	9.5975(8)	10.275(6)	14.007(3)
<i>c</i> /Å	23.079(3)	19.067(2)	24.980(2)	11.844(7)	18.935(3)
α (°)	90	93.895(2)	90	70.91(1)	103.999(4)
β (°)	90	94.406(2)	90	83.27(2)	91.508(4)
γ (°)	90	104.332(2)	90	89.32(2)	96.957(4)
<i>V</i> /Å ³	2025.9(5)	1042.5(2)	1198.5(2)	724.3(7)	2548.5(8)
<i>Z</i>	8	2	4	2	6
<i>T</i> /K	293(2)	296(2)	296(2)	296(2)	293(2)
<i>F</i> (000)	880	412	800	332	1092
ρ /g cm ⁻³	1.381	1.237	2.358	1.487	1.354
μ /mm ⁻¹	0.344	0.100	0.104	0.273	0.214
Scan technique	ω and φ	ω and φ	ω and φ	ω and φ	ω and φ
Data collected	(-11, -9, -18) to (15, 9, 27)	(-7, -8, -22) to (7, 10, 22)	(-6, -11, -30) to (6, 9, 30)	(-7, -12, -11) to (7, 10, 14)	(-11, -12, -22) to (11, 16, 22)
θ range (°)	1.76 to 27.00	1.08 to 25.00	1.63 to 26.00	1.83 to 25.00	1.11 to 25.00
Reflections collected	11 540	7996	9617	5594	19 528
Independent reflections	2138 (<i>R</i> _{int} = 0.0912)	3571 (<i>R</i> _{int} = 0.0391)	2343 (<i>R</i> _{int} = 0.0313)	2489 (<i>R</i> _{int} = 0.0959)	8734 (<i>R</i> _{int} = 0.1040)
Completeness to maximum θ (%)	96.6	97.0	99.6	97.3	97.2
Data/restraints/parameters	2138/0/127	3571/0/246	2343/0/163	2489/0/192	8734/0/655
Observed reflections [<i>I</i> > 2 σ (<i>I</i>)]	943	1749	2244	1029	2671
<i>R</i> ^a	0.0428	0.0619	0.0199	0.0641	0.0614
<i>R</i> _w ^b	0.1024	0.2181	0.0475	0.1681	0.1153

^a $\sum[|F_o| - |F_c|]/\sum|F_o|$. ^b $\{\sum[w(F_o^2 - F_c^2)^2]/\sum[w(F_o^2)^2]\}^{1/2}$.

compounds **BF₄-8** and **OTf-8**), which suggests the presence of strong H-bond interactions in solution.²⁹

As an interesting feature, it was remarkable to observe the influence of both factors, the counterion nature and the solution concentration, on the chemical shifts of aromatic and pyrazolium ring protons. Thus, we carried out two additional experiments. In the first, a ¹H-NMR study at a constant concentration (*C* = 6.7 × 10⁻³ M) was performed for all the salts containing 8 carbon atoms in the alkyl chain. In general, the signals in the aromatic region were down-field shifted with respect to those of the neutral pyrazole compounds.²⁴ This deshielding is counterion-dependent, the shift of the closest proton to the 1-NH pyrazolic nitrogen atom being the most modified one. As depicted in Table 3, the presence of BF₄⁻, OTf and PTS anions produced larger modifications in the pyrazolium signals than those observed for

**Scheme 4** Synthesis of the pyrazolium compounds I–VI.**Table 2** Nomenclature and formulation of the compounds described in the work^a

Family	I	II	III	IV	V	VI
Type	[H ₂ pz ^{R(n)}][Cl]	[H ₂ pz ^{R(n)}][BF ₄]	[H ₂ pz ^{R(n)}][ReO ₄]	[H ₂ pz ^{R(n)}][SbF ₆]	[H ₂ pz ^{R(n)}][OTf]	[H ₂ pz ^{R(n)}][PTS]
<i>n</i> = 1	Cl-1		ReO ₄ -1		OTf-1	PTS-1
<i>n</i> = 8	Cl-8	BF ₄ -8	ReO ₄ -8	SbF ₆ -8	OTf-8	PTS-8
<i>n</i> = 10	Cl-10	BF ₄ -10	ReO ₄ -10	SbF ₆ -10	OTf-10	PTS-10
<i>n</i> = 12	Cl-12	BF ₄ -12	ReO ₄ -12	SbF ₆ -12	OTf-12	PTS-12
<i>n</i> = 14	Cl-14	BF ₄ -14	ReO ₄ -14	SbF ₆ -14	OTf-14	PTS-14
<i>n</i> = 16	Cl-16	BF ₄ -16	ReO ₄ -16	SbF ₆ -16	OTf-16	PTS-16
<i>n</i> = 18	Cl-18	BF ₄ -18	ReO ₄ -18	SbF ₆ -18	OTf-18	PTS-18

^a R(*n*) = C₆H₄OC_nH_{2n+1}; OTf = CF₃SO₃⁻; PTS = CH₃-*p*-C₆H₄SO₃⁻.

the Cl^- , ReO_4^- and SbF_6^- salts. A similar fact has also been found for related alkyloxybenzyl-methyl-imidazolium based ionic liquid crystals,¹¹ and has been explained in terms of the different morphology and ability of the anion to interact with the cationic moiety, highlighting that these protons are very environment-sensitive.

In the second experiment, concentration-dependance studies were carried out for representative compounds (Table 4). When the concentration was increased, a down-field shift of the signals was generally observed, which could be attributed to the presence of aggregates in solution, as was observed in related cases.^{11,12,16} These variations are of a different magnitude depending on the counterion present in each salt.

The IR spectra of all salts in the solid state show the characteristic bands of the pyrazolium moiety as well as those of the corresponding counterions, where appropriate. In particular, the $\nu(\text{C}=\text{N}) + \nu(\text{C}=\text{C})$ and $\nu(\text{NH})$ absorption bands from the pyrazolium cation appear at *ca.* 1600 and in the 3100–3400 cm^{-1} range, respectively.³³ Additionally, characteristic bands of the counter-anions are also observed. In particular, for BF_4^- , ReO_4^- and SbF_6^- salts, bands at *ca.* 1080, 900 and 650 cm^{-1} corresponding to $\nu(\text{BF})$, $\nu(\text{ReO})$ and $\nu(\text{SbF})$ from the corresponding anions,³³ appear at values that agree with the ionic nature of the salts (II–IV). Also, the presence of the counterions OTf and PTS (V–VI) is clearly confirmed by the two bands at *ca.* 1250 cm^{-1} , $\nu_{\text{as}}(\text{SO}_3)$, and 1030 cm^{-1} , $\nu_{\text{s}}(\text{SO}_3)$, for the former, and 1180 cm^{-1} , $\nu_{\text{as}}(\text{SO}_3)$, and 1020 cm^{-1} , $\nu_{\text{s}}(\text{SO}_3)$, for the latter.³³

Crystal structures of $[\text{H}_2\text{pz}^{\text{R}(1)}][\text{Cl}]$ (Cl-1), $[\text{H}_2\text{pz}^{\text{R}(10)}][\text{BF}_4]$ (BF₄-10), $[\text{H}_2\text{pz}^{\text{R}(1)}][\text{ReO}_4]$ (ReO₄-1), $[\text{H}_2\text{pz}^{\text{R}(1)}][\text{OTf}]$ (OTf-1) and $[\text{H}_2\text{pz}^{\text{R}(1)}][\text{PTS}]$ (PTS-1)

The **BF₄-10** salt from family **II** is proven to produce crystals of sufficient quality for single-crystal X-ray analysis. However, for the remaining compounds, **I** and **III–VI**, all attempts to grow crystals were unsuccessful. We then tried to prepare and crystallise related salts of cationic species containing one methoxyphenyl substituent at the 3(5) position of the pyrazole ring, which, as expected, crystallise more easily than compounds containing long-chained cations. Therefore, crystals of **Cl-1**, **ReO₄-1**, **OTf-1** and **PTS-1** were obtained by slow vapour diffusion of *n*-hexane into a dichloromethane solution of the corresponding compound, and were characterised by single crystal X-ray diffraction.

The molecular structure of **Cl-1**, **BF₄-10**, **ReO₄-1**, **OTf-1** and **PTS-1** as representative examples of families **I**, **II**, **III**, **V** and **VI** are shown in Fig. 1–5. The bond lengths and angles are recovered

Table 3 Chemical shifts in the aromatic region for the salts containing 8 carbon atoms in the substituent alkyl chain at a constant solution concentration of 6.7×10^{-3} M

[A]	H5	H4	H _{ortho}	H _{meta}
Cl^-	7.91	6.72	7.94	7.02
BF_4^-	8.08	6.82	7.68	7.03
ReO_4^-	7.93	6.79	7.72	7.04
SbF_6^-	7.87	6.74	7.63	7.01
OTf	8.10	6.79	7.70	7.03
PTS	8.05	6.70	7.73	6.97

Table 4 Chemical shifts in the aromatic region for representative examples of the salts containing 8 carbon atoms in the substituent alkyl chain at various solution concentrations

Compound	C/mol L ⁻¹	H5	H4	H _{ortho}	H _{meta}
Cl-8	6.7×10^{-2}	7.90	6.71	7.93	7.01
	6.7×10^{-3}	7.91	6.72	7.94	7.02
	6.7×10^{-4}	7.91	6.72	7.94	7.02
BF₄-8	3.4×10^{-2}	8.14	6.81	7.68	7.02
	6.7×10^{-3}	8.08	6.82	7.68	7.03
	8.4×10^{-5}	7.92	6.83	7.65	7.05
OTf-8	3.3×10^{-2}	8.12	6.78	7.70	7.02
	6.7×10^{-3}	8.10	6.79	7.70	7.03
	1.7×10^{-3}	8.08	6.79	7.69	7.03
	3.3×10^{-4}	7.96	6.80	7.67	7.03

in Table S1–S5 (see ESI†). Table 5 lists the hydrogen bond geometries of these compounds.

Compound **BF₄-10** crystallises into the triclinic system, space group $P\bar{1}$. The crystal structure consists of dimers containing two cations and two anions held by $\text{N}\cdots\text{F}$ H-bonding interactions (Table 5), with both cations in a head to tail arrangement (Fig. 1). Columns of dimers are built along the *b* axis and consist of superposed rows of pyrazolium rings and single rows of BF_4^- anions, held together through conventional $\text{N}\cdots\text{F}$ and weak $\text{C}\cdots\text{F}$ H-bonding interactions (Table 5). Additional, very weak, $\text{C}\cdots\text{H}\cdots\text{F}$ interactions of 3.45 Å could be suggested as evidence supporting a potential 2D structure. The bond distances in the pyrazole and benzene rings are evidence of a delocalised π system (Table S1†). Additionally, they show a high degree of planarity, as deduced from the dihedral angles of $4.1(1)^\circ$ between both rings.

The crystal packing of **BF₄-10** is shown in Fig. 6. The supramolecular arrangement is typical of a layered structure with alternation of polar groups and hydrophobic chains. In the layer the chains exhibit a *trans* orientation giving rise to a highly interdigitated structure along the *c* axis. The long molecular axis of the cation is tilted with respect to the normal layer. The interlayer separation is 19.1(1) Å.

The straight-chain nature of the alkyl groups is maintained along the structure with carbon chain torsion angles approaching 180° . The chain configuration and the lack of any disorder in the structure appear to be a consequence of the interdigitated molecular packing. The formation of separate hydrophilic and hydrophobic structural parts has been proved to be useful for the formation of liquid-crystalline phases.¹⁷

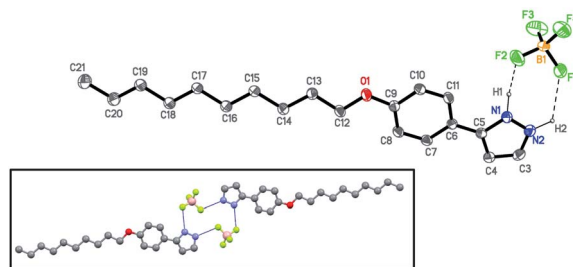


Fig. 1 Ortep plot of $[\text{H}_2\text{pz}^{\text{R}(10)}][\text{BF}_4]$ **BF₄-10** with 30% probability. Hydrogen atoms, except H1 and H2, have been omitted for clarity. The dimer structure is depicted in the inset.

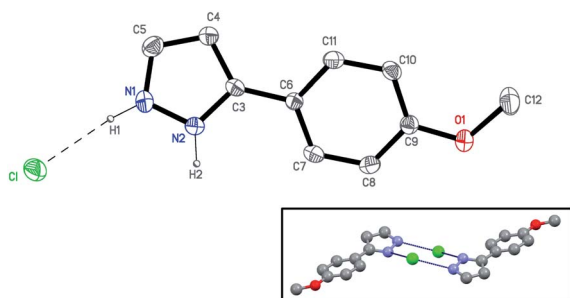


Fig. 2 Ortep plot of $[\text{H}_2\text{pz}^{\text{R}(1)}][\text{Cl}]$ **Cl-1** with 40% probability. Hydrogen atoms, except H1 and H2, have been omitted for clarity. The dimer structure is depicted in the inset.

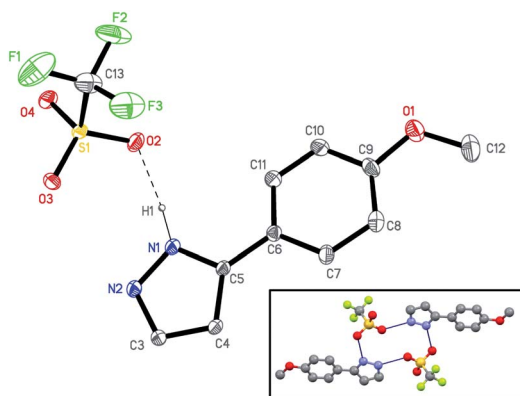


Fig. 3 Ortep plot of $[\text{H}_2\text{pz}^{\text{R}(1)}][\text{OTf}]$ **OTf-1** with 20% probability. Hydrogen atoms, except H1, have been omitted for clarity. The dimer structure is depicted in the inset.

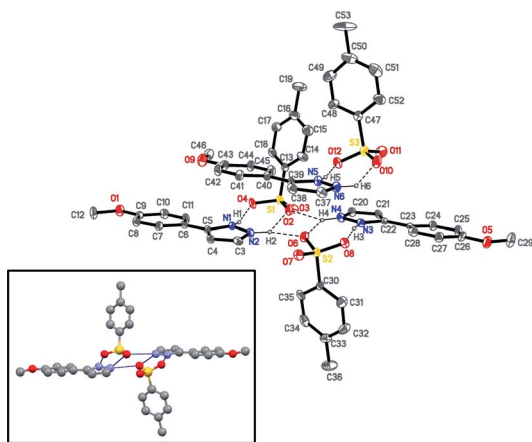


Fig. 4 Ortep plot of $[\text{H}_2\text{pz}^{\text{R}(1)}][\text{PTS}]$ **PTS-1** with 30% probability. Hydrogen atoms, except H1, H2, H3, H4, H5 and H6, have been omitted for clarity. The dimer structure is depicted in the inset.

The single crystal X-ray structures of representative compounds of families **I**, **V** and **VI** show that **Cl-1** crystallises into the orthorhombic system, group $Pbca$, while **PTS-1** and **OTf-1** crystallises into the triclinic one, group $P(\bar{1})$. The compounds **Cl-1** and **OTf-1** present one cation and one anion in the asymmetric unit, while three cations and three anions are observed for **PTS-1** (Fig. 2–4). Bond lengths and angles are well

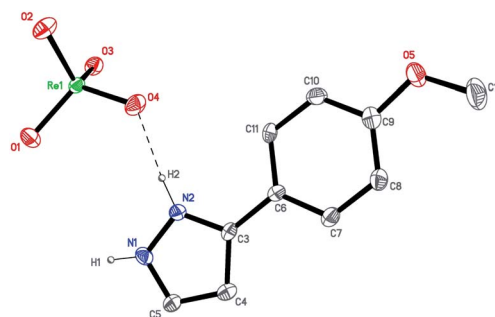


Fig. 5 Ortep plot of $[\text{H}_2\text{pz}^{\text{R}(1)}][\text{ReO}_4]$ **ReO4-1** with 30% probability. Hydrogen atoms, except H1 and H2, have been omitted for clarity.

within the expected range (Tables S2–S4†). The pyrazolium head group and the phenyl substituent are almost in the same plane for **PTS-1** and **OTf-1** as they were observed in the **BF4-10** derivative. However, both planes are tilted by $21.5(1)^\circ$ for **Cl-1**. Following the alternation of the polar and hydrophobic parts found for **BF4-10**, the $[\text{H}_2\text{pz}^{\text{R}(1)}]^+$ cation present in the three salts can be considered as containing a hydrophilic part (the pyrazolium group) and a hydrophobic methyl group from the *p*-methoxyphenyl substituent, which are in close proximity. The cations are bonded to their corresponding anions by $\text{N-H}\cdots\text{X}$ H-bonds ($\text{X} = \text{O}$ for **PTS-1** and **OTf-1**, Cl for **Cl-1**) and, in the three cases, dimers held by $\text{N-H}\cdots\text{X}$ H-bonds between neighbouring units are formed (Table 5; Fig. 2–4). From this point, similar structural packing features were found for **PTS-1** and **OTf-1**, but were different from those of the **Cl-1** salt. In **PTS-1** and **OTf-1**, columns of dimers are defined from weak $\text{C-H}\cdots\text{O}$ interactions, but a 2D arrangement is obtained for **Cl-1** through additional $\text{C-H}\cdots\text{O}$ H-bonds.

The columns in **PTS-1** and **OTf-1** are arranged in layer-like arrays. The layers in the *ac* and *ab* planes, respectively (Fig. 7 and Fig. S1†), can be defined as holding together rows of the cationic part of the pyrazolium and the SO_3 rows of the triflate or *p*-toluenesulfonate groups in **OTf-1** and **PTS-1**, respectively. The remaining fragments, CF_3 from the triflate and $\text{C}_6\text{H}_4\text{OCH}_3$ from the *p*-toluenesulfonate, are located each side of the layer pointing out in opposite directions and are tilted towards the main plane of the layer.

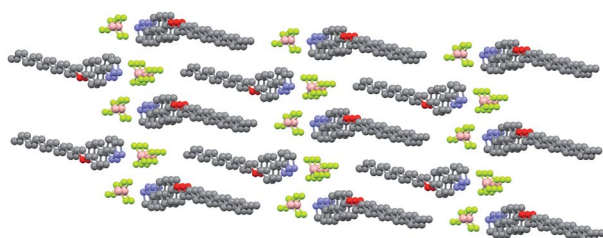
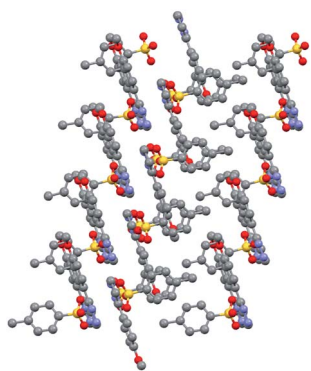
The molecular structure of **Cl-1** is displayed in Fig. 2. As was mentioned, the $[\text{H}_2\text{pz}^{\text{R}(1)}]^+$ cation exhibits similar structural characteristics to those presented in the related salts with OTf or PTS, except for the dihedral angle between the pyrazolium and benzene rings. So, each cation is NH-bonded to its chlorine anion, and is again NH-bonded to the neighbouring unit, generating bridge-chlorine dimers in which the $\text{Cl}\cdots\text{N}$ are practically identical (Table 5; Fig. 2). However, in this case, in contrast to that observed for **OTf-1** and **PTS-1**, each dimer is surrounded another four and is bonded to them by weak $\text{C-H}\cdots\text{O}$ interactions between the central carbon atom of the pyrazolium ring and the oxygen of the methoxy group, generating a corrugated layer which is extended in the *ac* plane (Fig. 8). The layers are separated from one another by a distance of 5.4 Å, and no short contacts were found between layers.

The supramolecular 2D structure of the chlorine salts of the $[\text{H}_2\text{pz}^{\text{R}(1)}]^+$ cation was clearly different to those of the related salts with OTf, PTS or BF_4^- , which by contrast exhibit a similar layer-like array of columns of cations and anions. For the latter

Table 5 Hydrogen bond geometries (lengths in Å and angles in degrees) for **Cl-1**, **BF₄-10**, **ReO₄-1**, **OTf-1** and **PTS-1**

Compound	D–H···A	d(D–H)	d(H···A)	d(D···A)	<(D–H···A)
Cl-1	N1–H1···Cl	0.92	2.11	3.019(3)	172.4
	N2–H2···Cl ^a	0.92	2.16	3.055(2)	163.6
	C4–H4···O1 ^b	0.93	2.57	3.32(1)	138.4
BF₄-10	N1–H1···F2	1.05	1.77	2.805(4)	166.8
	N2–H1···F1 ^c	1.08	1.77	2.774(4)	151.7
	C3–H3···F4 ^d	0.93	2.40	3.28(1)	158.0
ReO₄-1	N2–H2···O4	0.90	1.88	2.751(6)	163.2
	N1–H1···O3 ^e	0.96	1.78	2.703(6)	160.2
	C5–H5···O3 ^d	0.93	2.44	3.20(1)	138.1
OTf-1	N1–H1···O2	1.05	1.76	2.791(5)	166.6
	N2–H2···O3 ^f	1.04	1.89	2.817(5)	147.2
	C4–H4···O4 ^d	0.93	2.46	3.38(1)	171.0
PTS-1	N1–H1···O4	0.98	1.82	2.752(6)	156.7
	N2–H2···O6	0.97	1.90	2.790(6)	151.0
	N3–H3···O8	1.09	1.67	2.754(5)	170.3
	N4–H4···O2	1.00	1.93	2.767(6)	140.1
	N5–H5···O12	1.04	1.73	2.757(6)	165.3
	N6–H6···O10 ^g	0.94	1.91	2.741(6)	146.4
	C38–H38···O11 ^h	0.93	2.35	3.24(1)	160.4
	C21–H21···O7 ⁱ	0.93	2.37	3.28(1)	163.3

^a $-x+1, -y+2, -z+1$. ^b $x-1/2, y, -z+1/2$. ^c $-x-1, -y+1, -z+1$. ^d $x, y+1, z$. ^e $x+1/2, -y+1/2, -z$. ^f $-x, -y+1, -z+2$. ^g $-x, -y+1, -z+1$. ^h $x+1, y, z$. ⁱ $x-1, y, z$.

**Fig. 6** Packing of **BF₄-10** in the *bc* plane.**Fig. 7** Packing of **PTS-1** in the *bc* plane.

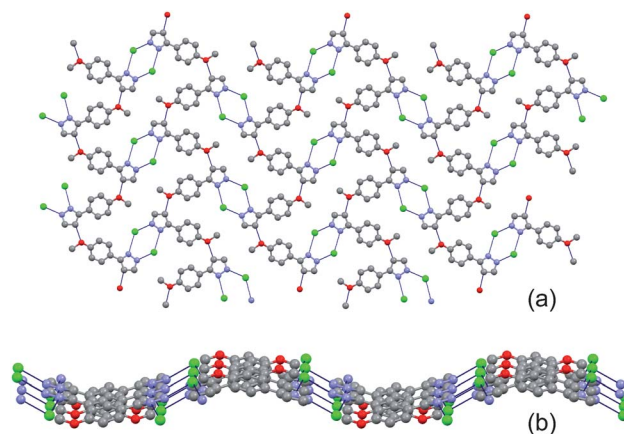
groups of salts, the interlayer distance was determined by the anion, and the longest distances were produced by the bulkiest anions (OTf, PTS).

Compound **ReO₄-1** crystallises into the orthorhombic system, space group $P2_12_12_1$. The asymmetric unit contains a crystallographically independent cation $[H_2pz^{R(1)}]^+$ and an ReO_4^- anion (Fig. 5).

The bond lengths and angles in the organic cations are broadly within the expected range (Table S5[†]) and can be compared to

the ones, in the long or short chain pyrazolium compounds, previously mentioned. In the same way as in the previous salts, each cation is strongly H-bonded to its own ReO_4^- counter-anion, but this unit does not produce dimers as in the previous salts. In contrast, the pyrazolium cations and ReO_4^- anions form double chains by stacking along the *a* axis through N–H···O H-bonds involving two NH groups per cation and two oxygen atoms per anion (Table 5). In each double chain, the cations stack in such a way that the methoxyphenyl substituents alternate in orientation, giving rise to a herringbone-type chain structure (Fig. 9). These double chains form a layer-like array in the *ac* plane, in which neighbouring chains have opposite distributions showing a clear interdigitation (Fig. 9).

In addition, a 2D bilayer structure can be defined in the *ab* plane by new weak C–H···O interactions between chains. The cations are oriented in a such way that an angle of 44.6° is adopted between the bilayer plane and the benzene plane. The

**Fig. 8** View of the 2D structure of **Cl-1** (a) in the *ac* plane and (b) in the *bc* plane.

bilayer thickness is 15 Å and the separation between neighbouring bilayers is 12.5 Å, suggesting certain interpenetration.

The above structures can be extrapolated to those of related long-chained ionic salts $[H_2pz^{R(n)}][A]$ ($n = 8-18$), so that the H-bonds responsible for the layer-like structure for BF_4^- salts, and even the 2D structures in Cl^- and ReO_4^- derivatives, can be considered as an important factor for achieving the supramolecular ordering of the fluid phases observed in the mentioned ionic salts (see below). However, the anion size and the morphology also play an important role, in such a way that the bulkiest PTS and OTf anions prevent the supramolecular arrangement of the fluid phases.

Thermal behaviour

The thermal behaviour of all the new ionic compounds was examined by polarised optical microscopy (POM) and differential scanning calorimetry (DSC). A detailed temperature-dependent, low-angle powder X-ray diffraction study was also performed for representative compounds of each family.

All the pyrazolium salts **I-IV** with $n = 8-18$ show enantiotropic SmA mesophases, except the compound **Cl-8** which exhibits a monotropic SmA mesophase (Table 6). In contrast, neither of the salts **V** or **VI** display liquid crystal behaviour (Table S6†), which is consistent with the absence of mesomorphism observed in related imidazolium-based ionic liquid compounds containing bulky counteranions.^{5,13,16,18}

The mesomorphic behaviour observed in compounds **I-IV** shows significant differences with that of some other related salts. For instance, the melting and clearing temperatures were higher than those of 1-alkyl-3-methylimidazolium and 1-(4-alkyloxybenzyl)-3-methylimidazolium with the same counterions.^{3,4,11,14-16} The presence of H-bonding interactions, supported by the X-ray crystalline structures described above, appears to be responsible for the stabilization of the ordered phases.

Additionally, the mesomorphism of pyrazolium salts containing Cl^- as counterion (**I**) contrasts with that of related salts containing a pyridinium head, for which protonation on the heterocyclic nitrogen and the presence of the Cl^- counterion constituted an impediment to acquiring liquid crystal properties.^{22,23}

All the compounds **I-VI** exhibit a rich polymorphism, showing several crystalline phases deduced from the DSC thermograms and POM observations.

In all cases, the mesophases were undoubtedly recognised as SmA on the basis of their optical textures. During the cooling

process from the isotropic liquid, the formation of *bâtonnets* was observed, which, upon further cooling, gave rise to a fan-shaped texture together with homeotropic areas (Fig. 10a-c). In addition, during heating, the formation of oily streaks upon deformation of the samples confirms the identification of the mesophase (Fig. 10d).

For the salts, including those with OTf (**V**) and PTS (**VI**) as counteranions, the phase transition temperatures from the solid to the isotropic liquid are increased by lowering the alkyl chain length, indicating that the higher mobility of the longer substituents disrupts the van der Waals interactions.

On heating, the DSC thermograms of compounds **I-IV** revealed large enthalpy values for the Cr-Cr' and Cr-SmA phase transitions, as well as small enthalpy values which were consistently observed for the SmA-I phase transitions. The related reverse transitions on cooling exhibited the same behaviour and are assigned to the I-SmA, SmA-Cr and Cr-Cr' phase transitions. A typical DSC thermogram of a mesomorphic compound, **Cl-10**, is shown in Fig. 11.

In general terms, all members of each mesomorphic family (**I-IV**) exhibit a similar pattern upon heating and cooling with the exception of **ReO₄-10**, **ReO₄-12** and **ReO₄-14** compounds for which the phase transition involving solidification from the mesophase could not be observed neither by the DSC thermograms nor by POM observations. Further POM, DSC and powder X-Ray diffraction experiments were carried out in order to achieve new results. A description of the particular study of these compounds is now presented.

New DSC thermograms of **ReO₄-10**, **ReO₄-12** and **ReO₄-14** were recorded after heating the samples just above the melting point and then cooling down from this temperature. In this way, we were able to register an endothermic peak related to the mesophase-solid phase transition, in agreement with the solid phase observed by POM upon cooling from the mesophase when the same thermal route was used. We also carried out new POM studies by modifying the experimental conditions, as are now described for **ReO₄-12**. A sample of this compound was slowly cooled down at 1 °C min⁻¹ from the liquid, in 20 °C steps, holding the temperature for several hours after each step. The formation of a solid phase was observed at 90 °C after 18 hours. A sample of the same compound was heated to the isotropic phase and then quenched to room temperature, giving rise to a solid phase, considered as a supercooled phase, which maintained the mesophase texture. Analogous temperature programs were followed for X-Ray diffraction measurements in order to confirm the existence of different final phases depending on the cooling rate, which will be described later.

At this point of the manuscript, for a better understanding of the thermal behaviour each type of compound and for comparative purposes, we are going to present the results for each family (**I-IV**).

I (Cl-n): all the chloride salts displayed enantiotropic mesomorphism with exception of compound **Cl-8** which exhibited a monotropic mesophase. The melting and clearing temperatures showed only small variations, including a slight increase in the liquid crystal range with increasing alkyl chain length from $n = 10$ until $n = 14$ and a decrease for $n > 14$. Thus, the compound of the family with the widest mesophase range is **Cl-14** (Fig. 12a).

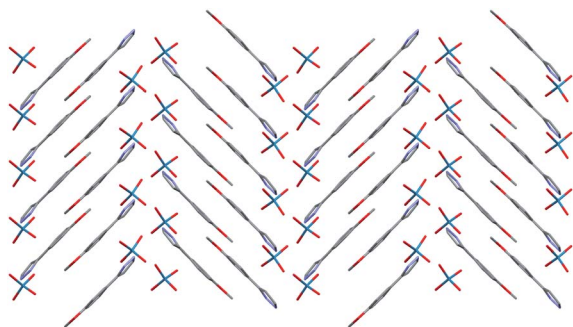


Fig. 9 Packing of the ReO_4-1 in the ac plane.

Table 6 Thermal data of compounds of the families I (Cl-*n*), II (BF₄-*n*), III (ReO₄-*n*) and IV (SbF₆-*n*)^a

Compound	Transition	<i>T</i> /°C	ΔH /kJ mol ⁻¹	Compound	Transition	<i>T</i> /°C	ΔH /kJ mol ⁻¹
Cl-8	Cr → I	150	30.6	ReO₄-8	Cr → Cr'	124	27.2
	I → SmA	150	-2.4		Cr' → SmA	155	23.2
	SmA → Cr	139	-14.7		SmA → I	164	2.0
Cl-10	Cr → SmA	150	23.1	ReO₄-10	I → SmA	162	-2.0
	SmA → I	166	2.1		SmA → Cr	113	-22.8
	I → SmA	157	-1.6		Cr → SmA	118	44.0
	SmA → Cr	135	-12.5		SmA → I	190	1.7
	Cr → Cr'	97	-3.0		I → SmA	183	-0.9
Cl-12	Cr → SmA	144	27.1	ReO₄-12	SmA → Cr	64 ^c	-28.3
	SmA → I	170	1.9		Cr → SmA	118	53.6
	I → SmA	168	-1.7		SmA → I	208	1.1
Cl-14	SmA → Cr	133	-21.4	ReO₄-14	I → SmA	206	-0.7
	Cr → SmA	140	32.8		SmA → Cr	78	-40.3 ^b
	SmA → I	170	1.5		Cr → Cr'		
Cl-16	I → SmA	162	-1.1	ReO₄-16	Cr → SmA	114	43.0
	SmA → Cr	128	-16.5		SmA → I	195	0.6
	Cr → Cr'	99	-4.4		I → SmA	189	-0.5
	Cr → SmA	140	41.0		SmA → Cr	70	-38.8
	SmA → I	167	1.7		Cr → Cr'	87	3.6
Cl-18	I → SmA	148	-0.8	ReO₄-18	Cr' → SmA	112	45.0
	SmA → Cr	123	-14.0		SmA → I	162	0.6
	Cr → Cr'	105	-8.7		I → SmA	162	-0.5
	Cr → SmA	138	43.7		SmA → Cr	108	-7.4
	SmA → I	166	1.3		Cr → Cr'	61	-23.9
BF₄-8	I → SmA	158	-0.8	SbF₆-8	Cr → SmA	113	67.4
	SmA → Cr	129	-25.3		SmA → I	148	0.3
	Cr → Cr'	103	-5.7		I → SmA	147	-0.2
	Cr → SmA	86	17.0		SmA → Cr	104	-10.5
	SmA → I	110	1.0		Cr → Cr'	78	-25.4
BF₄-10	I → SmA	106	-1.0	SbF₆-10	Cr → Cr'	100	0.2
	SmA → Cr	80	^d		Cr' → Cr''	112	0.2
	Cr → Cr'	80	12.7		Cr'' → SmA	147	11.8 ^b
	Cr' → SmA	123	25.2		SmA → I		
	SmA → I	165	1.4		I → SmA	144	-0.6
BF₄-12	I → SmA	162	-1.5	SbF₆-12	SmA → Cr	80	-3.1
	SmA → Cr	100	-31.4		Cr → Cr'	91	2.8
	Cr → Cr'	91	10.8		Cr' → Cr''	104	20.0
	Cr' → SmA	122	23.8		Cr'' → SmA	151	17.6 ^b
	SmA → I	182	1.0		SmA → I		
BF₄-14	I → SmA	181	-1.0	SbF₆-14	I → SmA	144	-14.2 ^b
	SmA → Cr	87	-33.8		SmA → Cr		
	Cr → Cr'	98	13.5		Cr → Cr'	91	-18.7
	Cr' → SmA	122	28.6		Cr → Cr'	114	25.1
	SmA → I	187	1.0		Cr' → SmA	153	26.8 ^b
BF₄-16	I → SmA	186	-0.9	SbF₆-16	SmA → I		
	SmA → Cr	91	-39.2		I → SmA	142	-1.3
	Cr → SmA	104	62.3		SmA → Cr	132	-25.1
	SmA → I	179	0.4		Cr → Cr'	88	-19.1
	I → SmA	175	-0.7		Cr → Cr'	113	31.3
BF₄-18	SmA → Cr	90	-53.5	SbF₆-18	Cr' → SmA	144	27.9
	Cr → Cr'	78	-2.2		SmA → I	166	1.0
	Cr → SmA	102	63.7		I → SmA	155	-0.4
	SmA → I	162	0.2		SmA → Cr	100	-16.1
	I → SmA	144	-0.2		Cr → Cr'	87	-13.2
	SmA → Cr	81	-69.7	Cr → Cr'	118	49.4 ^b	
				Cr' → SmA	129		
				SmA → I	209	dec.	
				Cr → Cr'	121	72 ^b	
				Cr' → SmA	132		
				SmA → I	199	0.5	
				I → SmA	175	-0.5	
				SmA → Cr	99	-37.9	

^a Temperatures from the DSC peak. ^b Overlapped processes. ^c Solidification observed on the second heating process. ^d Temperature given by POM.

II (BF₄-*n*): in this family the melting temperatures are lower than those observed for the related Cl⁻ salts and again, they were almost unmodified by increasing the alkyl chain length (except

BF₄-8), but showed a slight decrease for long-tailed derivatives. In contrast, the clearing temperatures increased significantly until *n* = 14 and then they decreased. As a consequence, the

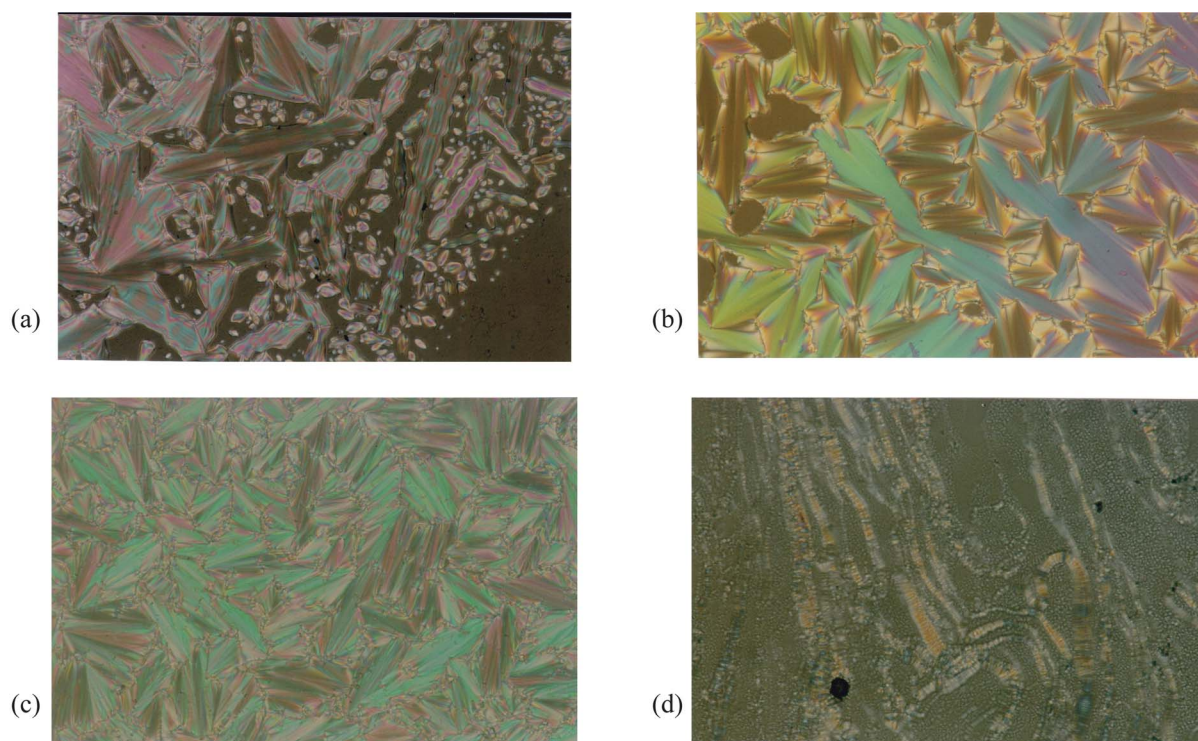


Fig. 10 POM photomicrographs of: (a) **BF₄-8** at 102.0 °C during cooling; (b) **ReO₄-12** at 195.0 °C during cooling; (c) **SbF₆-18** at 138.3 °C during cooling; (d) **Cl-18** at 147.0 °C during heating.

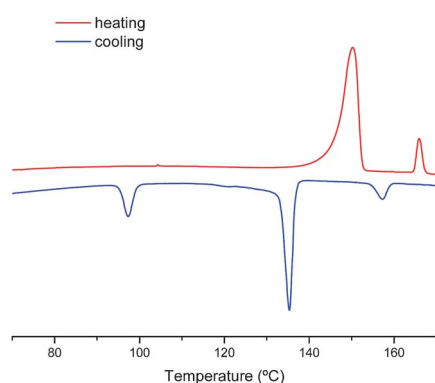


Fig. 11 DSC trace for **Cl-10**.

mesophase range reaches the highest value for the compound **BF₄-16** (Fig. 12b).

III (ReO₄-n): the melting points of the compounds of this series are, in general terms, slightly lower than those observed for the analogue **BF₄⁻** salts and follow the same pattern by the increasing the alkyl chain length. However, the clearing points depend strongly on this variable, giving rise to a mesophase stability range which reaches the highest value for the compound **ReO₄-12** (Fig. 12c).

IV (SbF₆-n): the clearing and melting temperatures are close to those of the **Cl⁻** salts, although for the longest alkyl chain substituted compounds the liquid crystalline range expands due to a slight decrease of the melting temperatures and a significant increase of the clearing points, leading to wider mesophase ranges for compounds **SbF₆-16** and **SbF₆-18** (Fig. 12d).

Two effects were taken into account in order to discuss the different thermal behaviour of the compounds **I–IV**: the effect of the counterion and the effect of the alkyl chain length. Considering the effect of the counterion on the transition temperatures, we found that the geometry and size seem to modulate the melting temperatures of the new salts. The spherical or quasi-spherical **Cl⁻** and **SbF₆⁻** anions give rise to higher melting points in their salts (**I** and **IV**), which is consistent with a more favourable packing in the solid state. In contrast, the salts containing the tetrahedral **BF₄⁻** and **ReO₄⁻** anions (**II** and **III**) exhibit lower melting temperatures as a consequence of an apparently less favoured packing (Fig. 12). The anion size was also important, with the bulkiest ones giving rise to the lowest melting temperatures. So, considering both effects, the melting temperatures were found to be in the order $\text{ReO}_4^- \leq \text{BF}_4^- < \text{SbF}_6^- < \text{Cl}^-$ for a given cation (Fig. 12).

Regarding the clearing transition, the compounds **I** and **IV**, containing spherical anions, exhibit, in general terms, lower clearing temperatures than those of the related derivatives **II** and **III**, with tetrahedral anions. This fact suggests an increase in the cation–cation electrostatic repulsions for the first case. Among the latter (**II** and **III**), the bulky **ReO₄⁻** group should disrupt the cationic proximity more easily, therefore decreasing the cationic repulsion and so giving rise to higher clearing temperatures. However, this feature was observed only in the compound family **III** when $n \leq 14$ carbon atoms in the hydrophobic tail, while for longer chains an opposite variation was exhibited.

When studying the effect of the alkyl chain length, some features have been determined. As the first, compounds containing alkyl chains with $n = 8$ appear to deviate from the general trend, as is shown by the monotropic behaviour of **Cl-8** or the

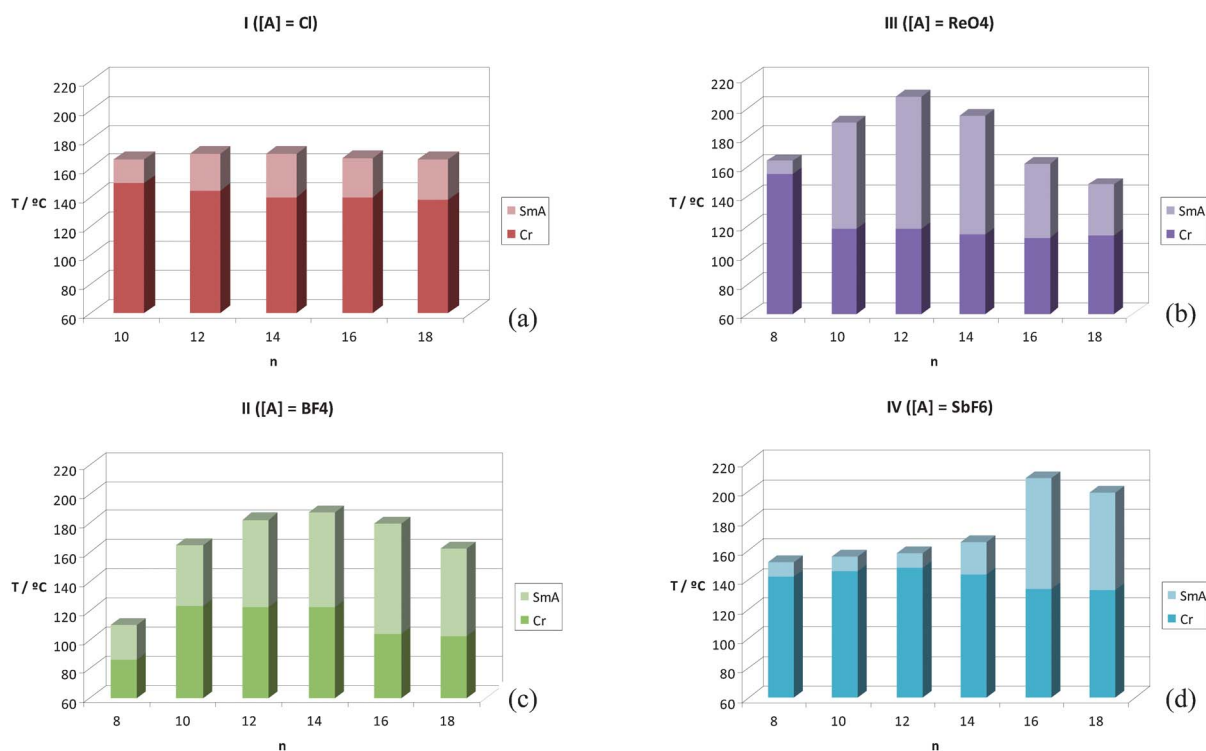


Fig. 12 Bar diagram comparing the stability ranges of mesophases for each family.

mesophase ranges exhibited by **BF₄-8** and **ReO₄-8**, which are narrower than those of the remaining derivatives in their families. This feature suggests that the driving forces for the formation of the liquid crystalline state require a chain length of $n \geq 8$ to be optimised. As we commented, in the remaining compounds, the melting temperatures seem to be modulated by the anion shape and size while the clearing points are governed by both counteranion nature and cation length. Thus, for cations containing short chains ($n = 10, 12, 14$), the lowest melting temperatures and the highest clearing temperatures, and so the widest mesophase ranges, correspond to the salts with tetrahedral anions, **BF₄⁻** and **ReO₄⁻** (Fig. 13a–c). However, going to the longest cation-containing compounds, with $n = 16$ and 18 , the clearing temperatures remain almost constant for **Cl⁻** salts but tend to decrease for tetrahedral anion containing salts (showing an opposite variation in the order **BF₄⁻** > **ReO₄⁻**) and, finally, they are markedly increased in **SbF₆⁻** derivatives (Fig. 13d–e). For these longest compounds, as the melting temperatures are almost unaffected by the alkyl length growing, the widest mesophase ranges among long tailed salts are observed in **SbF₆⁻** derivatives.

Therefore, for the longest compounds, the van der Waals interactions between the hydrophobic tails over the electrostatic forces between ions in the mesophase must be a predominant effect. In contrast, the electrostatic repulsions appear to be determinant in compounds with the shortest chain lengths, yielding higher clearing points for salts containing tetrahedral anions. The singular order of the clearing temperatures, **SbF₆⁻** > **BF₄⁻** > **ReO₄⁻**, found for long-tailed derivatives, requires an additional explanation, which emerges by considering the influence of the hydrogen bonding as a support of the interactions that should contribute to govern the mesophase.

In summary, taking into account all the above results we can establish that the best results for the mesophase emerging and its stability are found for compounds in the order **ReO₄-12** and **ReO₄-14** > **BF₄-16** and **BF₄-18** \geq **SbF₆-16** and **SbF₆-18**.

In relation to ionicity of the studied systems, the evidence of the liquid crystal behaviour established for the pyrazolium salts, **[H₂pz^{R(m)}][A]**, which, by contrast was absent in their corresponding neutral pyrazoles, **Hpz^{R(m)}**, exclude the dissociation of the protonated cationic form, at least in certain extension. The establishment of this premise should be a motive for new studies taking into account results previously described.^{34,35}

Temperature-dependent powder X-ray diffraction studies

Selected mesomorphic derivatives of families **I–IV** were subjected to temperature-dependent powder X-ray diffraction (XRD) measurements. In all cases, the XRD patterns at the mesophase temperature show, in the low-angle region, two to four sharp peaks in a 1 : 2 : 3 : 4 ratio indexed as the (001), (002), (003) and (004) reflections, which are indicative of a lamellar structure. In addition, a broad halo in the medium-angle region, at *ca.* 4.5 Å corresponds to the liquid-like order of the molten alkyl chains. The results are summarised in Table 7. Fig. 14 shows the diffraction pattern of compound **ReO₄-16** as a representative example.

An interesting feature was observed by comparing the layer spacing of compounds with equal alkyl chain lengths and different counterions. A longer layer spacing was observed for **ReO₄-8** than that of its homologue, **BF₄-8**, in agreement with the larger size of the perrhenate anion. This result appears to confirm the proposal concerned with the higher clearing points found for **ReO₄⁻** salts due to the lower cationic proximity in the mesophase.

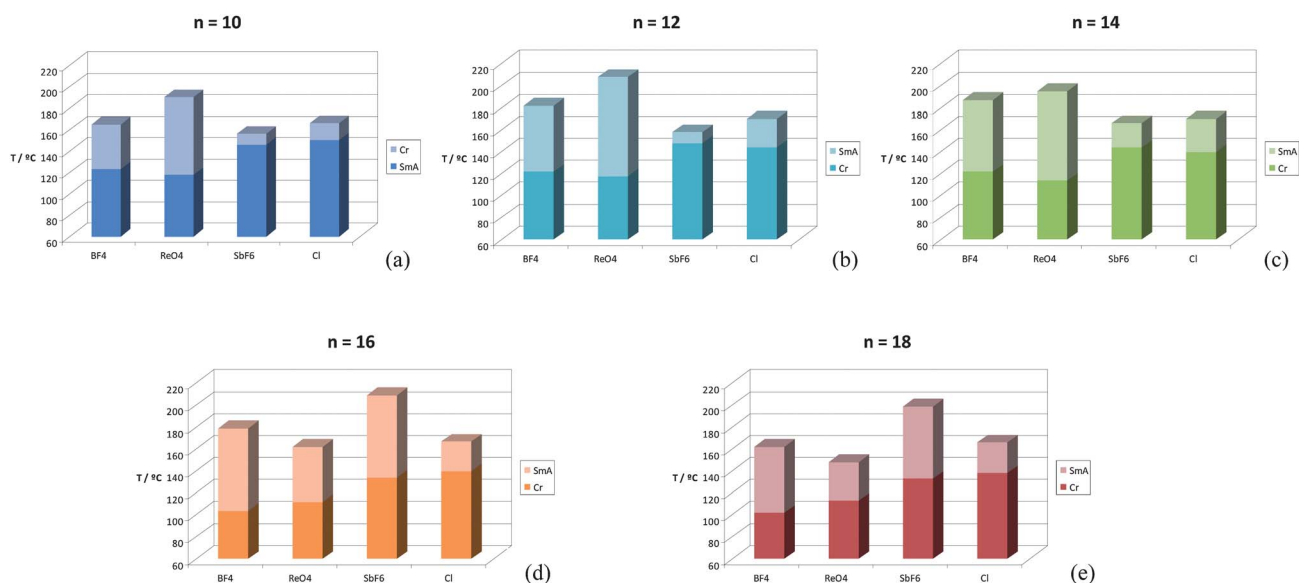


Fig. 13 Bar diagram comparing the stability ranges of mesophases for each carbon atom in the chain.

Because of the singular behaviour of perrhenate derivatives upon cooling, we carried out a further XRD study for **ReO₄-12** as a representative example, following analogous temperature programs to those used in the POM observations (see thermal behaviour section). In an initial experiment, a sample was slowly cooled down (1 °C min⁻¹) to room temperature (25 °C) after reaching the isotropic liquid phase (215 °C). The diffraction patterns obtained each 10–20 °C were characteristic of a smectic mesophase until 90 °C. However, upon further cooling from this temperature, the intensity of the sharp peaks at the low angle region gradually decreased and finally disappeared at 25 °C in agreement with the formation of an amorphous solid phase at

room temperature. In a second experiment, a sample was quenched to room temperature from the isotropic phase. In that case, the diffractogram at 25 °C, showing 3 sharp peaks at the low angle region, and a broad halo in the middle angle region, was characteristic of a smectic mesophase, suggesting the presence of a supercooled mesophase. This feature agrees with the POM observation of a fan-shape texture at room temperature after following a similar cooling cycle.

Conclusions

New mesomorphic compounds based on long alkyl chain-substituted pyrazolium cations with different counterions have been prepared and characterised as mesomorphic materials. We have established that the melting temperatures are modulated by the shape of the counterion while both the size and shape of the anion and the length of the alkyl chain should be considered for the clearing temperatures. The spherical or pseudo spherical shape of Cl⁻ and SbF₆⁻ anions determines a favourable packing in the solid and a cation–cation proximity in the mesophase, which leads to higher melting temperatures but lower clearing

Table 7 X-Ray diffraction data of selected compounds

Comp.	T/°C ^a	Position/2θ	d-spacing/Å	Miller indices (hkl)
Cl-18	135	2.3	38.7	(001)
		4.5	19.5	(002)
		18.5	4.8	^b
BF ₄ -8	90	3.0	29.4	(001)
		6.0	14.7	(002)
		19.5	4.5	^b
ReO ₄ -8	140	2.8	31.6	(001)
		5.3	16.7	(002)
		7.9	11.1	(003)
		10.6	8.3	(004)
		20.7	4.3	^b
ReO ₄ -12	130	2.6	34.5	(001)
		4.7	18.9	(002)
		7.0	12.6	(003)
		9.4	9.4	(004)
		19.5	4.5	^b
ReO ₄ -16	140	2.3	38.7	(001)
		4.4	19.9	(002)
		20.1	4.4	^b
SbF ₆ -10	150	2.4	36.5	(001)
		4.8	18.4	(002)
		18.9	4.7	^b

^a Upon cooling. ^b Halo of the molten alkyloxy chains.

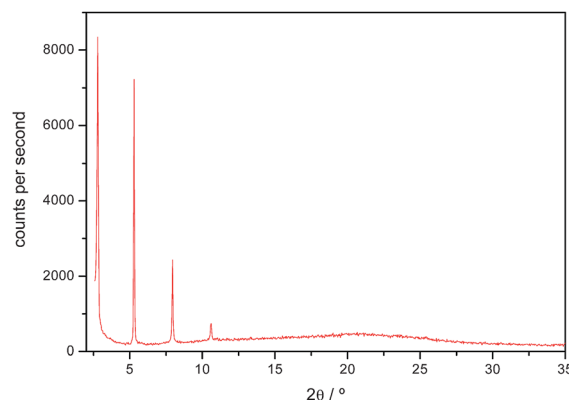


Fig. 14 X-Ray diffraction pattern of compound ReO₄-16.

temperatures, respectively. The opposite effect is observed in the derivatives containing the tetrahedral BF_4^- and ReO_4^- anions. In those compounds, the van der Waals interactions between chains are in competition with the electrostatic effects depending on the size of the counterions as well as the alkyl chain length. In particular, the use of tetrahedral anions, ReO_4^- combined with cations containing alkyl chains with 10 to 14 carbon atoms or BF_4^- bonded to long-chained substituted cations ($n > 14$), produce better results than the use of spherical or quasi spherical Cl^- and SbF_6^- anions.

Structural relationships between the solid phase and the mesophase have been found. The pyrazolium ionic salts exhibited 2D or layer-like crystalline structures defined by strong and weak hydrogen bond interactions, which can be related to those of the lamellar mesophases observed in the Cl^- , BF_4^- and ReO_4^- salts. The bulkiest anions, OTf and PTS, expanded the thickness of the layers by their CF_3 or $\text{C}_6\text{H}_4\text{CH}_3$ groups, respectively, included laterally side by side. As a consequence, there is difficulty in achieving the H-bonding interactions responsible for the supra-molecular ordering of the fluid phases, which results in the absence of mesomorphism for these OTf and PTS derivatives. In contrast, the 2D, layered, crystalline structures of the ReO_4^- salts agree with the best liquid crystal properties. Nevertheless, the corrugated 2D, layered structure of Cl^- derivatives seems to be responsible for less extensive liquid crystal ranges in these salts.

Acknowledgements

We thank the Ministerio de Economía y Competitividad (Spain), projects CTQ2010-19470 and CTQ2011-25172, and Universidad Complutense de Madrid (Spain), project GR35/10-A-910300, for financial support. I. S. thanks the Ministerio de Educación (Spain) for the predoctoral scholarship from the FPU program.

Notes and references

- P. Wasserscheid and W. Keim, *Angew. Chem., Int. Ed.*, 2000, **39**, 3773; K. R. Seddon, *J. Chem. Technol. Biotechnol.*, 1997, **68**, 351; T. Welton, *Chem. Rev.*, 1999, **99**, 2071.
- I. J. B. Lin and Ch. S. Vasam, *J. Organomet. Chem.*, 2005, **690**, 3498.
- K. Binnemans, *Chem. Rev.*, 2005, **105**, 4148.
- K. V. Axenov and S. Laschat, *Materials*, 2011, **4**, 206.
- M. Yoshio, T. Ichikawa, H. Shimura, T. Kagata, A. Hamasaki, T. Mukai, H. Ohno and T. Kato, *Bull. Chem. Soc. Jpn.*, 2007, **80**, 1836.
- M. Yoshio, T. Mukai, H. Ohno and T. Kato, *J. Am. Chem. Soc.*, 2004, **126**, 994.
- T. Kato, N. Mizoshita and K. Kishimoto, *Angew. Chem., Int. Ed.*, 2006, **45**, 38.
- T. Welton, *Coord. Chem. Rev.*, 2004, **248**, 2459.
- W. Dobbs, J.-M. Suisse, L. Douce and R. Welter, *Angew. Chem., Int. Ed.*, 2006, **45**, 4179; A. Taubert and Z. Li, *Dalton Trans.*, 2007, 723; A. Taubert, C. Palivan, O. Casse, F. Gozzo and B. Schmitt, *J. Phys. Chem. C*, 2007, **111**, 4077; A. Taubert, I. Arbell, A. Mecke and P. Graf, *Gold Bull.*, 2006, **39**, 205; Q. T. Wang, X. B. Wang, W. J. Lou and J. C. Hao, *ChemPhysChem*, 2009, **10**, 3201.
- W. Dobbs, B. Heinrich, C. Bourgogne, B. Donnio, E. Terazzi, M.-E. Bonnet, F. Stock, P. Erbacher, A.-L. Bolcato-Bellemin and L. Douce, *J. Am. Chem. Soc.*, 2009, **131**, 13338.
- W. Dobbs, L. Douce and B. Heinrich, *Beilstein J. Org. Chem.*, 2009, **5**, 62.
- M. Trilla, R. Pleixats, T. Parella, C. Blanc, P. Dieudonné, Y. Guari and M. W. C. Man, *Langmuir*, 2008, **24**, 259.
- A. E. Bradley, C. Hardacre, J. D. Holbrey, S. Johnston, S. E. J. McMath and M. Nieuwenhuyzen, *Chem. Mater.*, 2002, **14**, 629.
- C. J. Bowlas, D. W. Bruce and K. R. Seddon, *Chem. Commun.*, 1996, 1625.
- C. M. Gordon, J. D. Holbrey, A. R. Kennedy and K. R. Seddon, *J. Mater. Chem.*, 1998, **8**, 2627; J. D. Holbrey and K. R. Seddon, *J. Chem. Soc., Dalton Trans.*, 1999, 2133.
- W. Dobbs, L. Douce, L. Allouche, A. Louati, F. Malbosc and R. Welter, *New J. Chem.*, 2006, **30**, 528.
- A. Getsis and A.-V. Mudring, *Cryst. Res. Technol.*, 2008, **43**, 1187.
- K.-M. Lee, Y.-T. Lee and I. J. B. Lin, *J. Mater. Chem.*, 2003, **13**, 1079.
- K. Goossens, K. Lava, P. Nockemann, K. Van Hecke, L. Van Meervelt, K. Driesen, C. Görller-Walrand, K. Binnemans and T. Cardinaels, *Chem.-Eur. J.*, 2009, **15**, 656.
- V. Causin and G. Saielli, *J. Mater. Chem.*, 2009, **19**, 9153.
- V. Causin and G. Saielli, *J. Mol. Liq.*, 2009, **145**, 41.
- E. J. R. Sudhölter, J. B. F. N. Engberts and W. D. de Jeu, *J. Phys. Chem.*, 1982, **86**, 1908.
- J. J. H. Nusselder, J. B. F. N. Engberts and H. A. Van Doren, *Liq. Cryst.*, 1993, **13**, 213.
- M. C. Torralba, M. Cano, J. A. Campo, J. V. Heras, E. Pinilla and M. R. Torres, *J. Organomet. Chem.*, 2001, **633**, 91.
- M. C. Torralba, M. Cano, J. A. Campo, J. V. Heras, E. Pinilla and M. R. Torres, *Inorg. Chem. Commun.*, 2002, **5**, 887.
- M. C. Torralba, M. Cano, J. A. Campo, J. V. Heras, E. Pinilla and M. R. Torres, *J. Organomet. Chem.*, 2002, **654**, 150; M. C. Torralba, M. Cano, S. Gómez, J. A. Campo, J. V. Heras, J. Perles and C. Ruiz-Valero, *J. Organomet. Chem.*, 2003, **682**, 26.
- M. C. Torralba, P. Ovejero, M. J. Mayoral, M. Cano, J. A. Campo, J. V. Heras, E. Pinilla and M. R. Torres, *Helv. Chim. Acta*, 2004, **87**, 250; M. C. Torralba, M. Cano, J. A. Campo, J. V. Heras and E. Pinilla, *Z. Kristallogr.-New Cryst. Struct.*, 2005, **220**, 615.
- M. J. Mayoral, P. Ovejero, J. A. Campo, J. V. Heras, E. Pinilla, M. R. Torres, C. Lodeiro and M. Cano, *Dalton Trans.*, 2008, 6912.
- M. J. Mayoral, P. Ovejero, J. A. Campo, J. V. Heras, M. R. Torres, C. Lodeiro and M. Cano, *New J. Chem.*, 2010, **34**, 2766.
- J. Barberá, C. Cativiela, J. L. Serrano and M. M. Zurbano, *Liq. Cryst.*, 1992, **11**, 887.
- M. J. Mayoral, P. Ovejero, J. A. Campo, J. V. Heras, E. Pinilla, M. R. Torres and M. Cano, *Inorg. Chem. Commun.*, 2009, **12**, 214.
- G. M. Sheldrick, SHELX97, *Program for Refinement of Crystal Structure*, University of Göttingen, Göttingen, Germany, 1997.
- K. Nakamoto, *Infrared and Raman Spectra of Inorganic and Coordination Compounds*, John Wiley & Sons, New York, 5th edn, 1986.
- D. R. MacFarlane and K. R. Seddon, *Aust. J. Chem.*, 2007, **60**, 3.
- D. R. MacFarlane, J. M. Pringle, K. M. Johansson, S. A. Forsyth and M. Forsyth, *Chem. Commun.*, 2006, 1905.